Letter Vol. 43, No. 13 / 1 July 2018 / Optics Letters 3017

Optics Letters

Diaphragm-free gas-pressure sensor probe based on hollow-core photonic bandgap fiber

ZHE ZHANG, JUN HE,* QI DONG, ZHIYONG BAI, CHANGRUI LIAO, YING WANG, SHEN LIU, KUIKUI GUO, AND YIPING WANG

Key Laboratory of Optoelectronic Devices and Systems of Ministry of Education and Guangdong Province, College of Optoelectronic Engineering, Shenzhen University, Shenzhen 518060, China

**Corresponding author: hejun07@szu.edu.cn*

Received 27 March 2018; revised 16 May 2018; accepted 23 May 2018; posted 24 May 2018 (Doc. ID 326962); published 18 June 2018

A diaphragm-free probe-type gas-pressure sensor is proposed and experimentally demonstrated based on a hollow-core photonic bandgap fiber (HC-PBF) with a quartz capillary. The section of the HC-PBF acts as a Fabry–Perot cavity, and the quartz capillary acts as a microfluidic channel for a gas inlet. An inner diameter of the quartz capillary (~2 μm) smaller than the HC-PBF (~10.9 μm) ensures a mirror reflection and a microfluidic channel simultaneously. The sensor probe has a minimal size (~125 μm) and can function at gas pressures as high as 8 MPa. A higher pressure test is limited by our gas-pressure generation devices. Excellent stability of the sensor is observed in a long time-scale, and repeatability of the sensor is confirmed by tests of six different samples. Compared with conventional optical fiber gas-pressure sensors, the proposed sensor involves a simple fabrication process and can acquire probe measurements with high sensitivity (~4.17 nm/MPa), excellent linearity (0.9999), fast response, and no hysteresis. The proposed sensor can also function at temperatures as high as 800°C, which is beneficial for high pressure measurements in extreme conditions. Moreover, the fast response of the sensor is attractive for dynamic pressure measurements, which needs further study and characterization.

OCIS codes: (060.2370) Fiber optics sensors; (060.5295) Photonic crystal fibers; (060.4005) Microstructured fibers.

https://doi.org/10.1364/OL.43.003017

The air core surrounding hollow-core bandgap fibers (HC-PBFs) offers an excellent platform for strong light-matter interactions over a long path length. Compared with other hollow-core fibers, such as hollow-core anti-resonance fibers [1], HC-PBFs guide light using the photonic bandgap effect and have a lower transmission loss as a result. The transmission loss of an HC-PBF is typically 1.2 dB/km [2], which is slightly larger than that of solid-core fibers. HC-PBFs have been demonstrated for a variety of applications in high-power laser pulse delivery and shaping [3], all-optical switching [4], particle guidance [5], single-photon memory [6], composition analysis of trace samples [7], gas sensing [8], and nonlinear optical methods such as cross-phase modulation [9] and Raman enhancement [10]. Several devices based on HC-PBFs have been developed such as long-period fiber gratings [11], in-fiber polarizers [12], polarization controllers [13], and in-fiber interferometers [14]. One of the most important applications of HC-PBFs involves their acting as a gas cell for the optical detection of gases. Previous studies have reported trace gas detection using HC-PBFs and gas absorption spectroscopy [15]. Recently, photo-thermal gas effects have been studied with an HC-PBF-based Fabry–Perot interferometer (FPI) [16]. This reduced the detection limits of trace gases down to hundreds of parts per billion [16]. FPIs, which typically employ a fiber-tip diaphragm cavity, have been studied extensively for gas-pressure measurements. A variety of diaphragm materials have been used, including silica [17], polymers [18], silver [19], and graphene [20].

Diaphragm-based FPI gas-pressure sensors typically measure the deformation of the diaphragm and can be made ultra-sensitive by employing a thin diaphragm with a low elastic modulus. However, thin diaphragms can only operate in limited gas-pressure ranges, on the order of hundreds of kilopascals. Additionally, the linearity, repeatability, and resilience of diaphragm-based sensors are generally poor due to mechanical deformations. Recently, fiber FPI gas-pressure sensors have been reported based on HC-PBFs using gas-pressure-induced refractive index (RI) change [21,22] or optical phase variation [23]. This new mechanism for gas-pressure measurements allows for high linearity, repeatability, resilience, and fast gas response.

However, the gas cavities reported in these studies included a hollow section in the fiber core area, and this hollow section functions poorly as an optical waveguide [21]. As a result, this limits the FPI cavity length, which determines the free spectral range (FSR) of the reflection spectrum and, hence, reduces the detection resolution [22]. The micro-channels for a gas inlet in previous studies have often been established by femtosecond laser drilling of lateral holes, which requires high-precision control of pulse energy, ablation time, and fiber position [22], This inevitably produces debris which results in transmission loss and affects the quality of interference spectra. Therefore, a longer FPI cavity which can improve the detection resolution and an excellent microfluidic channel for a gas inlet are in demand to improve the performance of optical fiber gas-pressure sensors.

This Letter proposes a diaphragm-free probe-type gas-pressure sensor based on an HC-PBF. The gas microfluidic channel is established by fusion splicing a quartz capillary with an inner diameter of ~2 μm at one end face of the HC-PBF. A gas-pressure test was conducted in the range of 0–8 MPa with a sensitivity of 4.17 nm/MPa and an ultrahigh linearity of 0.9999 at a wavelength of ~1560 nm. A test in a higher pressure range is limited by our pressure generation devices. In addition, the proposed sensor is compact and could further be developed into a portable sensing probe. The remainder of this Letter describes the fabrication of the device and experimentally demonstrates its viability for high-sensitivity gas-pressure measurements.

The structure of the proposed gas-pressure sensor probe is illustrated in Fig. 1(a). A section of HC-PBF was interposed between a lead-in single-mode fiber (SMF) and a quartz capillary using an arc discharge fusion splicer. The first reflection occurs at the interface of the SMF and HC-PBF, and the second reflection occurs at the interface of the HC-PBF and quartz capillary. The other end face of the quartz capillary is tilted and was produced by manually fracturing the quartz capillary to eliminate parasitic reflections from the end face. The employed HC-PBF was an "HC-1550-2" model with an air core of ~10.9 μm. The employed quartz capillary has an inner diameter of ~2 μm and a length of a few hundred microns. It should be noted that the quartz capillary acted as both a reflector and a microfluidic channel for a gas inlet. Capillaries with larger inner diameters will speed up the gas intake while reducing the reflection of the interface between the HC-PBF and quartz capillary. Hence, employing quartz capillaries with an inner diameter of 2 μm is a tradeoff between the speed of the gas intake and the intensity of the interface reflection. It should be noted that quartz capillaries with inner diameters larger than 10.9 μm will remove the second reflective interface of air and quartz and, hence, the FPI will no longer exist. Moreover, the low-loss transmission of an HC-PBF makes it possible to construct FPIs with longer cavities, resulting in an ultra-narrow 3 dB bandwidth, which is beneficial for wavelength demodulation. As such, an HC-PBF was chosen for this Letter, rather than other hollow-core fibers. Figure 1(b) shows a side-view microscopy image of the fabricated gas-pressure sensor probe. Figure 1(c) shows microscope images of the cross sections of the SMF, HC-PBF, and quartz capillary used in fabricating the gas-pressure sensor probe.

Six samples with varying FPI cavity lengths were fabricated, and their microscope images are shown in Fig. 2(a). The corresponding reflection spectra of the six fabricated samples were measured using a broadband light source, together with an optical spectrum analyzer (OSA), and the results are shown in Fig. 2(b). Moreover, longer HC-PBFs with narrower bandwidths were achievable, but not shown for the sake of brevity. The FPI cavity length and FSR of the six fabricated samples were recorded from Figs. 2(a) and 2(b), respectively, and demonstrated in the first two columns of Table 1. It is obvious that the FSR and FPI cavity lengths agree well with the following equation as

$$\mathrm{FSR} = \frac{\lambda^2}{2nL}, \tag{1}$$

where L is the cavity length, n is the RI of the cavity, and λ is the dip wavelength.

An experimental setup similar to that in our previous work was used to test the gas-pressure response of the proposed sensor probes [18]. Six samples with varying cavity lengths were encapsulated in the gas cell as pressure was gradually increased from 0 to 8 MPa with a step of 0.2 MPa. The dip wavelength in the reflection spectrum was traced using the OSA, and a linear "red shift" was observed as the pressure increased. The excellent resilience of this sensor was also demonstrated by the superposition of the traced dip wavelength when decreasing the

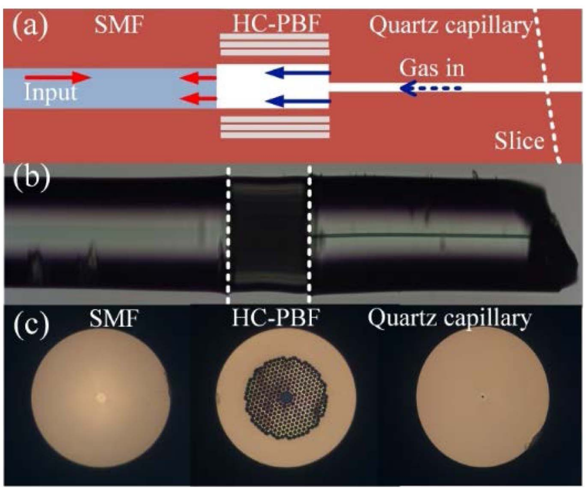

Fig. 1. (a) Schematic diagram of the proposed gas-pressure sensor probe. (b) Side-view microscope image of the fabricated gas-pressure sensor probe. (c) Microscope images of the cross section of the SMF (left), HC-PBF (middle), and quartz capillary (right).

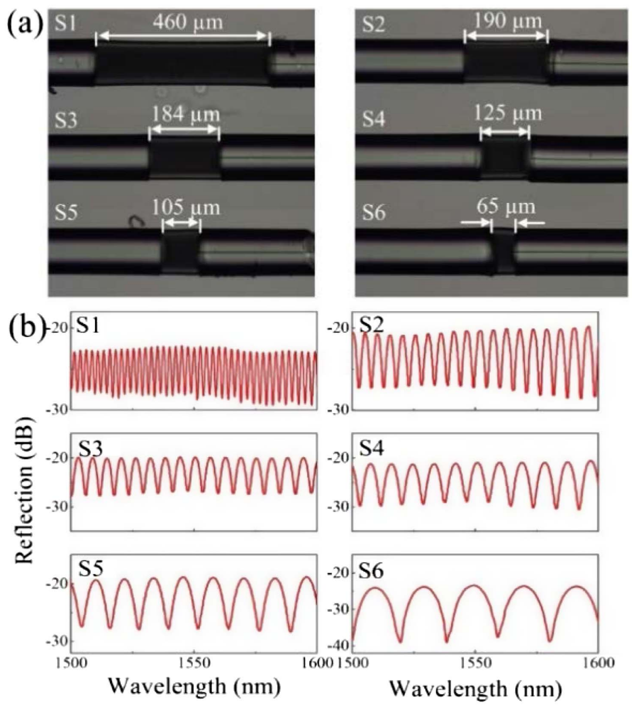

Fig. 2. (a) Microscope images of six different samples (S1-S6) fabricated with varying FPI cavity lengths. (b) Corresponding reflection spectra of the samples S1-S6, respectively.

pressure from 8 to 0 MPa with the same step. The response of the dip wavelength was rapid, with no hysteresis, and the linearity was ultrahigh due to pressure-induced RI variability. By employing a tunable laser, a photoelectric detector (PD), and an oscilloscope, we found that the response time of the sensor to gas-pressure change is less than 0.5 s. Figure 3 shows the wavelength response for one sample with a cavity length of ~190 μm, which resulted in a sensitivity of 4.17 nm/MPa and an ultrahigh linearity of 0.9999 at a wavelength of ~1560 nm. Sensitivities at different wavelengths are shown for a single sample in Fig. 4, and a comparison of all six samples is given in Table 1. These results demonstrate that sensor sensitivity is proportional to the traced wavelength and is independent of cavity length. This can be understood through a comparison with a theoretical calculation of sensitivity. Gas-pressure sensitivity can be expressed as

$$\frac{d\lambda}{dP} = \lambda\left(\frac{1}{L}\frac{dL}{dP} + \frac{1}{n}\frac{dn}{dP}\right). \tag{2}$$

As pressure increases, the RI of air in the cavity also increases [21]:

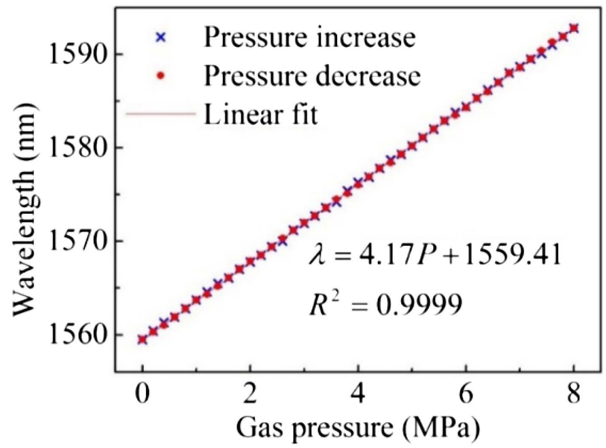

Fig. 3. Wavelength of the tracked dip plotted as a function of pressure.

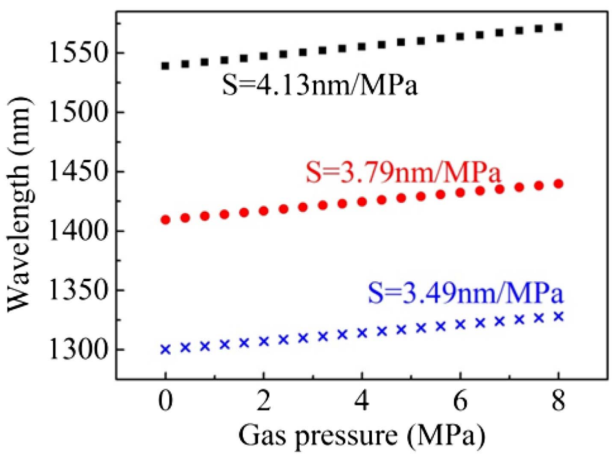

Fig. 4. Gas-pressure sensitivities for the same sample at varying wavelengths.

Table 1. Comparison of Samples with Varying FPI Cavity Lengths

Cavity Length	FSR (at ~1550 nm)	Sensitivity (at ~1550 nm)	R^2
65 μm	20.7 nm	4.17 nm/MPa	0.9998
105 μm	12.4 nm	4.36 nm/MPa	0.9999
125 μm	8.9 nm	4.20 nm/MPa	0.9998
184 μm	6.3 nm	4.17 nm/MPa	0.9999
190 μm	5.3 nm	4.13 nm/MPa	0.9999
460 μm	2.5 nm	4.19 nm/MPa	0.9997

$$n = 1 + \frac{2.8793 \times 10^{-9}}{1 + 0.00367 \times t}P, \tag{3}$$

where n, P, and t represent the RI of air, the pressure (Pa), and the temperature (°C), respectively. Compared with the side-opened HC-PBF channel, pressure-induced cavity length increments may be smaller in our case due to a reduced cross-sectional area [22]. Specifically, force on the outside HC-PBF surface remained constant. However, a larger area at both HC-PBF interfaces was under pressure as multiple HC-PBF cladding holes were formed by femtosecond laser ablation. As such, the contribution of cavity length to pressure sensitivity was smaller than 0.015 nm/MPa in this Letter, which is negligible compared to the sensor's sensitivity of 4.17 nm/MPa [22].

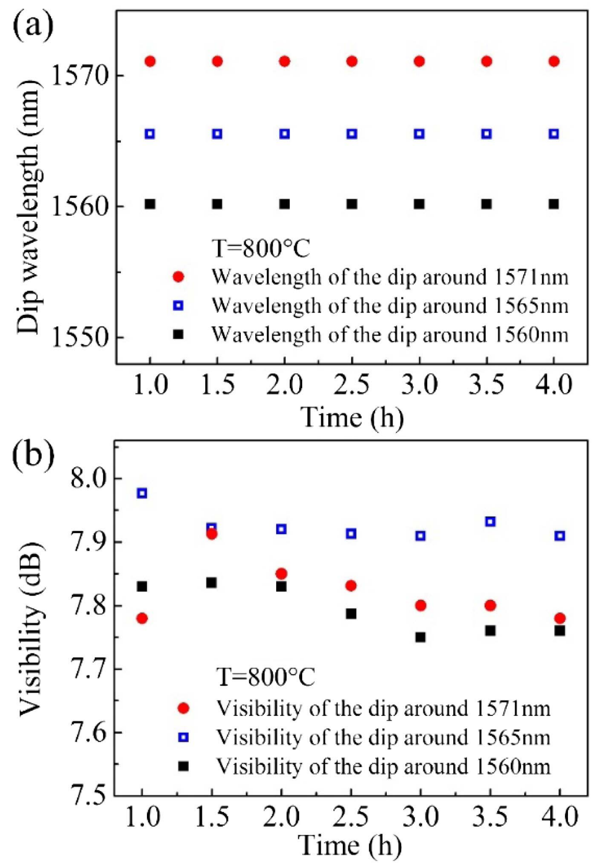

Fig. 5. (a) Wavelength and (b) visibility of three tracked dips at approximately 1571, 1565, and 1560 nm plotted as a function of heating time at 800°C.

Furthermore, it is obvious from Table 1 that the FPI cavity length has no effect on sensor sensitivity. However, FPIs with longer cavities can produce much narrower reflection dips and, hence, have better fineness, which benefits for wavelength demodulation resolution. By employing a wavelength demodulator with a high resolution of 0.1 pm, it is possible to achieve an extremely low pressure detection limit of ∼23 Pa. The sensor functioned at pressures higher than 8 MPa, which is beyond the range of our gas-pressure generator, and exhibited excellent resilience and linearity at these levels.

The all-silica structure of the proposed sensor also makes it a viable candidate for high-temperature operation. We employed an experimental setup similar to that in our previous work to test the performance of the sensor in high-temperature environments [24]. Three dip wavelengths were recorded by the OSA over the course of 4 h at a temperature of 800°C. This result is shown in Fig. 5, which demonstrates excellent thermal resistance. In addition, all three dip wavelengths shifted less than 1 nm while transitioning from room temperature (∼25°C) to 800°C, resulting in a temperature crosstalk of less than 1 kPa/°C. The insensitivity of this sensor to temperature changes may be attributed to low thermal expansion of the HC-PBF.

In summary, we proposed and demonstrated a diaphragm-free probe-type gas-pressure sensor based on an HC-PBF. A quartz capillary was utilized as both an FPI mirror and a microfluidic channel for a gas inlet, which avoids the disadvantages of microfluidic channels drilled by a femtosecond laser such as decries and high-precision control of pulse energy, ablation time, and fiber position. The proposed sensor structure has several advantages over conventional diaphragm deformation-based sensors, including excellent resilience, repeatability, linearity, and a large dynamic range. The stability of the sensor was also demonstrated experimentally, which could be beneficial for high temperature-pressure measurements. Moreover, the proposed sensor has a fast pressure response with hardly any hysteresis; the fast response of the sensor is attractive for dynamic pressure measurements, which needs further study and characterization. In addition, we believe the proposed structure is highly suitable for measuring the dispersion curves of functional fluids [25] in both biomedical and biochemical fields. Future research will explore the use of this sensor for these and other applications.

Funding. National Natural Science Foundation of China (NSFC) (61505120, 61425007, 61635007); Natural Science Foundation of Guangdong Province (2017A010102015, 2015A030310243, 2015B010105007, 2014A030308007); Science and Technology Innovation Commission of Shenzhen (JCYJ20170302143105991, JCYJ20170412105604705, JCYJ20160427104925452, JCYJ20160307143716576, JCYJ20170302154614941); Development and Reform Commission of Shenzhen Municipality Foundation.

REFERENCES

1. J. R. Hayes, F. Poletti, M. S. Abokhamis, N. V. Wheeler, N. K. Baddela, and D. J. Richardson, Opt. Express **23**, 1289 (2015).
2. P. J. Roberts, F. Couny, H. Sabert, B. J. Mangan, D. P. Williams, L. Farr, M. W. Mason, A. Tomlinson, T. A. Birks, J. C. Knight, and P. St.J. Russell, Opt. Express **13**, 236 (2005).
3. D. G. Ouzounov, F. R. Ahmad, D. Müller, N. Venkataraman, M. T. Gallagher, M. G. Thomas, J. Silcox, K. W. Koch, and A. L. Gaeta, Science **301**, 1702 (2003).
4. M. Bajcsy, S. Hoerberth, V. Balic, T. Peyronel, M. Hafezi, A. S. Zibrov, V. Vuletic, and M. D. Lukin, Phys. Rev. Lett. **102**, 203902 (2009).
5. F. Benabid, J. C. Knight, and P. St.J. Russell, Opt. Express **10**, 1195 (2002).
6. M. R. Sprague, P. S. Michelberger, T. F. M. Champion, D. G. England, J. Nunn, X.-M. Jin, W. S. Kolthammer, A. Abdolvand, P. St.J. Russell, and I. A. Walmsley, Nat. Photonics **8**, 287 (2014).
7. M. P. Buric, K. P. Chen, J. Falk, and S. D. Woodruff, Appl. Opt. **47**, 4255 (2008).
8. F. Yang, W. Jin, Y. Cao, H. L. Ho, and Y. P. Wang, Opt. Express **22**, 24894 (2014).
9. V. Venkataraman, K. Saha, and A. L. Gaeta, Nat. Photonics **7**, 138 (2012).
10. S. Hanf, T. Bögözi, R. Keiner, T. Frosch, and J. Popp, Anal. Chem. **87**, 982 (2014).
11. Y. P. Wang, W. Jin, J. Ju, H. F. Xuan, H. L. Ho, L. M. Xiao, and D. N. Wang, Opt. Express **16**, 2784 (2008).
12. H. F. Xuan, W. Jin, J. Ju, Y. P. Wang, M. Zhang, Y. B. Liao, and M. H. Chen, Opt. Lett. **33**, 845 (2008).
13. M. Pang and W. Jin, Opt. Lett. **36**, 16 (2011).
14. J. Ju, L. Ma, W. Jin, and Y. M. Hu, Opt. Lett. **34**, 1861 (2009).
15. E. Austin, A. V. Brakel, M. N. Petrovich, and D. J. Richardson, Sens. Actuators, B **139**, 30 (2009).
16. F. Yang, Y. Tan, W. Jin, Y. C. Lin, Y. Qi, and H. L. Ho, Opt. Lett. **41**, 3025 (2016).
17. C. R. Liao, S. Liu, L. Xu, C. Wang, Y. P. Wang, Z. Y. Li, Q. Wang, and D. N. Wang, Opt. Lett. **39**, 2827 (2014).
18. Z. Zhang, C. R. Liao, J. Tang, Z. Y. Bai, K. K. Guo, M. X. Hou, J. He, Y. Wang, S. Liu, F. Zhang, and Y. P. Wang, J. Lightwave Technol. **35**, 4067 (2017).
19. F. Xu, D. X. Ren, X. L. Shi, C. Li, W. W. Lu, L. Lu, L. Liang, and B. L. Yu, Opt. Lett. **37**, 133 (2012).
20. J. Ma, W. Jin, H. L. Ho, and J. Y. Dai, Opt. Lett. **37**, 2493 (2012).
21. M. Deng, C. P. Tang, T. Zhu, Y. J. Rao, L. C. Xu, and M. Han, Appl. Opt. **49**, 1593 (2010).
22. J. Tang, G. L. Yin, C. R. Liao, S. Liu, Z. Y. Li, X. Y. Zhong, Q. Wang, J. Zhao, K. M. Yang, and Y. P. Wang, IEEE Photon. J. **7**, 1 (2015).
23. Y. C. Cao, W. Jin, F. Yang, and H. L. Ho, Opt. Express **22**, 13190 (2014).
24. Z. Zhang, C. R. Liao, J. Tang, Y. Wang, Z. Y. Bai, Z. Y. Li, K. K. Guo, M. Deng, S. Q. Cao, and Y. P. Wang, IEEE Photon. J. **9**, 7101109 (2017).
25. C. L. Lee, H. Y. Ho, J. H. Gu, T. Y. Yeh, and C. H. Tseng, Opt. Lett. **40**, 459 (2015).